

A&A manuscript no.
(will be inserted by hand later)

Your thesaurus codes are:
06 (08.09.2 WR 1; 08.13.2; 08.23.2)

ASTRONOMY
AND
ASTROPHYSICS

January 20, 2018

An investigation of the large-scale variability of the apparently single Wolf-Rayet star WR 1

T. Morel^{1, *}, L. N. Georgiev², Y. Grosdidier^{1,3}, N. St-Louis¹, T. Eversberg^{1, **}, and G. M. Hill⁴

¹ Département de Physique, Université de Montréal, C. P. 6128, Succ. Centre-Ville, Montréal, Québec, Canada, H3C 3J7, and Observatoire du Mont Mégantic.

email: morel, yves, stlouis, eversber@astro.umontreal.ca

² Instituto de Astronomía, UNAM, Apdo. Postal 70-264, México D. F. 04510, México.

email:georgiev@astroscu.unam.mx

³ Observatoire Astronomique de Strasbourg, UMR 7550, 11 rue de l'Université, F-67000, Strasbourg, France.

⁴ McDonald Observatory, HET, P. O. Box 1337, Fort Davis, TX.

email:grant@astro.as.utexas.edu

Received ; accepted

Abstract. In recent years, much studies have focused on determining the origin of the large-scale line-profile and/or photometric patterns of variability displayed by some apparently single Wolf-Rayet stars, with the existence of an unseen (collapsed?) companion or of spatially extended wind structures as potential candidates. We present observations of WR 1 which highlight the unusual character of the variations in this object. Our narrowband photometric observations reveal a gradual increase of the stellar continuum flux amounting to $\Delta v \approx 0.09$ mag followed by a decline on about the same timescale (3-4 days). Only marginal evidence for variability is found during the 11 following nights. Strong, daily line-profile variations are also observed but they cannot be easily linked to the photometric variations. Similarly to the continuum flux variations, *coherent* time-dependent changes are observed in 1996 in the centroid, equivalent width, and skewness of He II $\lambda 4686$. Despite the generally coherent nature of the variations, we do not find evidence in our data for the periods claimed in previous studies. While the issue of a cyclical pattern of variability in WR 1 is still controversial, it is clear that this object might constitute in the future a cornerstone for our understanding of the mechanisms leading to the formation of largely anisotropic outflows in Wolf-Rayet stars.

Key words: Wolf-Rayet – WR 1 (HD 4004) – mass loss

Send offprint requests to: T. Morel

* *Present address:* Astrophysics Group, Imperial College of Science, Technology and Medicine, Blackett Laboratory, Prince Consort Road, London, SW7 2BZ, UK; email: t.morel@ic.ac.uk

** *Present address:* Feinfocus Medizintechnik GmbH, Im Bahlbrink 11-13, 30827, Garbsen, Germany; email: t.eversberg@feinfocus.com

Correspondence to: t.morel@ic.ac.uk

1. Introduction

It is now fairly well-established that *apparently single* Wolf-Rayet (WR) stars may display two distinct (but probably non mutually exclusive) spectroscopic patterns of variability: (a) small-scale emission features systematically moving from the line center to the line wings on an hourly timescale (e.g., Lépine 1998); (b) dramatically larger line-profile deformations operating on a much longer basis (\sim days, e.g., Smith & Willis 1994). Although the first phenomenon, observed in most (if not all) WR stars, is believed to be the consequence of the fragmented, possibly turbulent nature of the outflow, the origin of the latter type of variability is still very much elusive.

Remarkable in this respect, is the existence of a well-established (although strongly epoch-dependent) large-scale, *cyclical* pattern of variability in the two apparently single WR stars WR 6 ($\mathcal{P} = 3.763 \pm 0.002$ d; Firmani et al. 1980) and WR 134 ($\mathcal{P} = 2.27 \pm 0.04$ d; McCandliss et al. 1994; Morel et al. 1999). A major observational effort has been directed on establishing the true nature of these peculiar objects, i.e., whether this cyclical variability is induced by an orbiting unseen (collapsed?) companion or by the rotational modulation of large-scale wind structures (e.g., Vreux et al. 1992; Morel 1998; Harries et al. 1999, and references therein). Although the exact nature of these stars has yet to be unambiguously settled, these studies reveal that rotational modulation constitutes an attractive alternative to the binary hypothesis, especially considering the recent recognition that some O stars (the progenitors of WR stars) might possess such azimuthally structured outflows (Fullerton et al. 1997; Kaper et al. 1997).

A prime target for further investigations is the seldom-studied, apparently single WN 5 star WR 1 (HD 4004) that has recently been shown to present a spectral pattern of variability very similar to that of WR 6

(Niedzielski 1995, 1996a, b; Wessolowski & Niedzielski 1996; Niedzielski 1998). Strong line-profile variability was observed, as well as apparently cyclical (according to $\mathcal{P} \approx 2.667$ days) variations in the EWs of He II $\lambda 4686$ and He II $\lambda 5412$ (Niedzielski 1996a). The first claim of periodic variability in WR 1 with $\mathcal{P} \approx 7.7$ days was made by Lamontagne (1983) from an analysis of the radial velocity variations of He II $\lambda 4686$. The first photometric monitoring of this object has shown WR 1 to be variable, with an indication of a 6.1 day period (Moffat & Shara 1986). Recently, Marchenko et al. (1998a) discussed *Hip-parcos* broadband photometric data which revealed that WR 1 also displays relatively long-term photometric variations, with a marginal evidence for a $\mathcal{P} = 11.68 \pm 0.14$ day periodicity.

As can be seen, controversy persists in the literature concerning the possible cyclical nature of the variations in WR 1. We present in this paper the results of spectroscopic and photometric monitoring of WR 1 carried out in 1995 and 1996 aiming at shedding some light on this issue.

2. Observations and Reduction Procedure

2.1. Photometry

The photometric variability of WR 1 has been investigated during the interval 1996 September 18–October 5 by use of the single channel photometer *Cuentapulsos* on the 0.84 m telescope of the Observatorio Astronómico Nacional at San Pedro Mártir (Mexico). Two additional objects were monitored during this observing run, namely, WR 3 and WR 153. The nights were generally clear. WR 1 was observed through a narrowband v filter centered on 5140 Å (FWHM = 90 Å). This filter samples a continuum-dominated region of the WR spectrum. We applied the following sequence of 60 s integration through a 25'' diaphragm: sky, C2, C1, WR, C1, WR, C1, C2, sky. The same nearby comparison stars as used by Moffat & Shara (1986) have been chosen. These comparison stars are similar in terms of their magnitude and colour to WR 1: ΔB (WR – C1) = – 0.17, $\Delta[B - V]$ (WR – C1) = – 0.17, ΔB (WR – C2) = – 0.26, $\Delta[B - V]$ (WR – C2) = – 0.19. An extinction coefficient $k_v = 0.20$ was used throughout the data reduction. The scatter in the (C2 – C1) data for the whole dataset amounts to $\sigma = 4.7$ mmag. The differential magnitudes quoted in Table 1 are averaged over two consecutive cycles typically separated by about 20 minutes.

2.2. Spectroscopy

2.2.1. Long-slit and Reticon Spectra

Long-slit spectra of WR 1 have been obtained during various campaigns at the Observatoire du Mont Mégantic and Dominion Astrophysical Observatory (Canada) in 1995 October and 1996 September. Reticon spectra were also

obtained at DAO in 1996 November. The 1996 campaign at the Observatoire du Mont Mégantic was coordinated to support the photometric campaign described above. Table 2 lists the mode of observation, the dates of the spectroscopic observations, the interval of the observations in heliocentric Julian dates, the observatory name, the number of CCD spectra obtained, the selected spectral domain, the reciprocal dispersion of the spectra, and the typical signal-to-noise ratio (S/N) in the continuum. The spectra were reduced using the IRAF¹ data reduction packages. The bias and sky subtraction, flat-field division, removal of cosmic ray events, extraction of the spectra, and wavelength calibration were carried out in the usual way. Spectra of calibration lamps were taken immediately before and after the stellar exposure. The stellar spectra were subsequently continuum normalized by fitting a low-order Legendre polynomial to carefully selected line-free regions. In order to minimize the spurious velocity shifts induced by an inevitably imperfect wavelength calibration, the spectra were coaligned in velocity space by using the interstellar doublet Na I $\lambda\lambda 5890, 5896$ as fiducial marks. When not available, the doublet Ca II $\lambda\lambda 3934, 3968$ or the diffuse interstellar band at 4501 Å were used. A trend for a systematic shift of the zero point of the wavelength scale has been corrected by redshifting most of the spectra by an average value of 35 km s^{–1}.

2.2.2. Echelle Spectra

Echelle spectra have been obtained during the period 1996 September 16–19 with the Echelle spectrograph *Espresso* (Levine & Chakrabarty 1995) on the 2.1 m telescope of the San Pedro Mártir Observatory. The UCL camera and a 1024 × 1024 coated CCD-Tek chip have been used. The selected grating (300 lines mm^{–1}) yields a reciprocal dispersion of 0.16 and 0.23 Å pixel^{–1} at H γ and H α , respectively. The spectra cover 27 orders and span the spectral range 3720–6900 Å.

The reduction procedure (bias subtraction, division by a normalized flat field, removing of scattered light, extraction of the orders) was carried out using the reduction tasks in the IRAF package *echelle*. Comparison spectra of Th–Ar lamps have been used for the wavelength calibration. The typical accuracy of the wavelength calibration can be judged by the dispersion in the heliocentric radial velocities of the interstellar line Na I $\lambda 5890$: $\sigma \approx 2$ km s^{–1}. The instrumental response has been removed by fitting a low-order Legendre polynomial to the continuum sections of each order of an O-star spectrum, and then dividing the corresponding order of the WR 1 spectra by this polynomial. The resultant, almost flat orders were then combined

¹ IRAF is distributed by the National Optical Astronomy Observatories, operated by the Association of Universities for Research in Astronomy, Inc., under cooperative agreement with the National Science Foundation.

Table 1. Journal of photometric observations

HJD (− 2,449,000)	WR − C1	WR − C2	C2 − C1	HJD (− 2,449,000)	WR − C1	WR − C2	C2 − C1
1345.721	− 0.043	− 0.114	+ 0.071	1356.693	− 0.054	− 0.121	+ 0.067
1347.702	− 0.074	− 0.134	+ 0.061	1356.773	− 0.057	− 0.128	+ 0.071
1347.731	− 0.063	− 0.121	+ 0.058	1356.847	− 0.065	− 0.130	+ 0.065
1347.760	− 0.064	− 0.137	+ 0.073	1356.902	− 0.054	− 0.127	+ 0.073
1347.846	− 0.065	− 0.134	+ 0.069	1356.984	− 0.054	− 0.130	+ 0.076
1347.882	− 0.066	− 0.141	+ 0.075	1357.656	− 0.064	− 0.139	+ 0.075
1348.807	− 0.095	− 0.163	+ 0.068	1357.723	− 0.064	− 0.129	+ 0.065
1348.831	− 0.105	− 0.173	+ 0.067	1357.781	− 0.055	− 0.121	+ 0.066
1348.857	− 0.094	− 0.170	+ 0.076	1357.847	− 0.058	− 0.127	+ 0.070
1348.886	− 0.103	− 0.161	+ 0.058	1357.914	− 0.057	− 0.129	+ 0.072
1349.678	− 0.126	− 0.197	+ 0.071	1358.735	− 0.055	− 0.126	+ 0.071
1349.761	− 0.119	− 0.185	+ 0.066	1358.773	− 0.059	− 0.125	+ 0.066
1349.854	− 0.129	− 0.195	+ 0.065	1358.829	− 0.048	− 0.109	+ 0.061
1349.933	− 0.127	− 0.193	+ 0.065	1358.881	− 0.061	− 0.123	+ 0.062
1349.991	− 0.130	− 0.194	+ 0.064	1358.943	− 0.051	− 0.117	+ 0.066
1350.873	− 0.101	− 0.164	+ 0.063	1358.992	− 0.058	− 0.120	+ 0.062
1350.947	− 0.104	− 0.167	+ 0.063	1359.642	− 0.051	− 0.118	+ 0.067
1351.006	− 0.100	− 0.164	+ 0.064	1359.702	− 0.040	− 0.112	+ 0.072
1352.851	− 0.059	− 0.123	+ 0.064	1359.767	− 0.043	− 0.115	+ 0.071
1352.913	− 0.053	− 0.126	+ 0.073	1359.832	− 0.049	− 0.116	+ 0.067
1352.953	− 0.054	− 0.119	+ 0.065	1359.909	− 0.051	− 0.117	+ 0.066
1352.964	− 0.052	− 0.118	+ 0.066	1359.958	− 0.050	− 0.122	+ 0.072
1353.000	− 0.058	− 0.125	+ 0.067	1360.004	− 0.059	− 0.122	+ 0.063
1353.649	− 0.062	− 0.125	+ 0.063	1360.632	− 0.063	− 0.133	+ 0.070
1353.747	− 0.058	− 0.126	+ 0.067	1360.697	− 0.046	− 0.114	+ 0.067
1353.836	− 0.048	− 0.115	+ 0.067	1360.761	− 0.059	− 0.126	+ 0.067
1353.936	− 0.049	− 0.115	+ 0.066	1360.842	− 0.057	− 0.116	+ 0.060
1354.013	− 0.060	− 0.126	+ 0.066	1360.912	− 0.061	− 0.123	+ 0.062
1354.671	− 0.051	− 0.124	+ 0.073	1361.637	− 0.060	− 0.122	+ 0.061
1354.754	− 0.057	− 0.133	+ 0.076	1361.694	− 0.060	− 0.132	+ 0.073
1354.810	− 0.048	− 0.124	+ 0.076	1361.768	− 0.061	− 0.121	+ 0.060
1354.875	− 0.047	− 0.113	+ 0.066	1361.851	− 0.065	− 0.124	+ 0.060
1354.948	− 0.062	− 0.129	+ 0.067	1361.952	− 0.065	− 0.131	+ 0.066
1355.002	− 0.054	− 0.121	+ 0.068	1361.997	− 0.058	− 0.126	+ 0.069
1355.668	− 0.044	− 0.113	+ 0.070	1362.625	− 0.053	− 0.118	+ 0.066
1355.735	− 0.056	− 0.124	+ 0.068	1362.720	− 0.060	− 0.124	+ 0.064
1355.792	− 0.058	− 0.121	+ 0.063	1362.846	− 0.052	− 0.121	+ 0.069
1355.860	− 0.060	− 0.123	+ 0.063	1362.910	− 0.055	− 0.123	+ 0.068
1355.912	− 0.050	− 0.121	+ 0.071	1362.983	− 0.053	− 0.123	+ 0.070
1355.993	− 0.064	− 0.116	+ 0.052				

Table 2. Journal of spectroscopic observations

Mode of Observation	Date	HJD (− 2,449,000)	Observatory ^a	Number of Spectra	Spectral Coverage (Å)	Reciprocal Dispersion (Å pix ^{−1})	S/N
Long-slit	95 Oct	992-1005	OMM, DAO	7	3830-4300	1.6	≈ 160
				15	4360-5080	1.6	≈ 170
				11	5050-5945	1.6	≈ 290
Echelle	96 Sep	1342-1345	SPM	72	3720-6900	0.16 (H _γ) — 0.23 (H _α)	≈ 25 (H _γ) — 50 (H _α)
Long-slit	96 Sep	1346-1352	OMM	13	4400-5080	1.3	≈ 120
				14	5050-6500	1.3	≈ 190
Reticon	96 Nov	1386-1389	DAO	12	5100-6110	0.5	≈ 75

^a OMM: Observatoire du Mont Mégantic 1.6 m; DAO: Dominion Astrophysical Observatory 1.8 m; SPM: San Pedro Mártir Observatory 2.1 m.

using the IRAF task `scomb`. This procedure proved to be satisfactory, except when the overlapping regions fall in a spectral domain with very steep intensity gradients, as in the blue wing of He II $\lambda 4686$ (see Fig.2). The combined spectra were then subdivided into spectral regions roughly corresponding to those of the long-slit spectra discussed above (§2.2.1). For consistency purposes, these spectra have been continuum normalized by fitting a low-order Legendre polynomial to the *same* continuum sections that selected for the long-slit spectra.

3. Results

3.1. Photometric Variations

The light curve of WR 1 is plotted as a function of the heliocentric Julian date of observation in Figure 1. The main feature of this light curve is the gradual increase of the stellar continuum flux amounting to $\Delta v \approx 0.09$ mag beginning at HJD 2,450,346, followed by its decline on about the same timescale after HJD 2,450,350. During the last 11 nights (after HJD 2,450,353), only marginal evidence for variability is found, with $\sigma(\text{WR} - \text{C})/\sigma(\text{C2} - \text{C1}) \approx 1.3$. This can be compared with a value of 1.9 derived by Moffat & Shara (1986) on the basis of 14 nights of broadband *B* observations in 1984. Noticeable is the striking lack of recurrence in the continuum flux

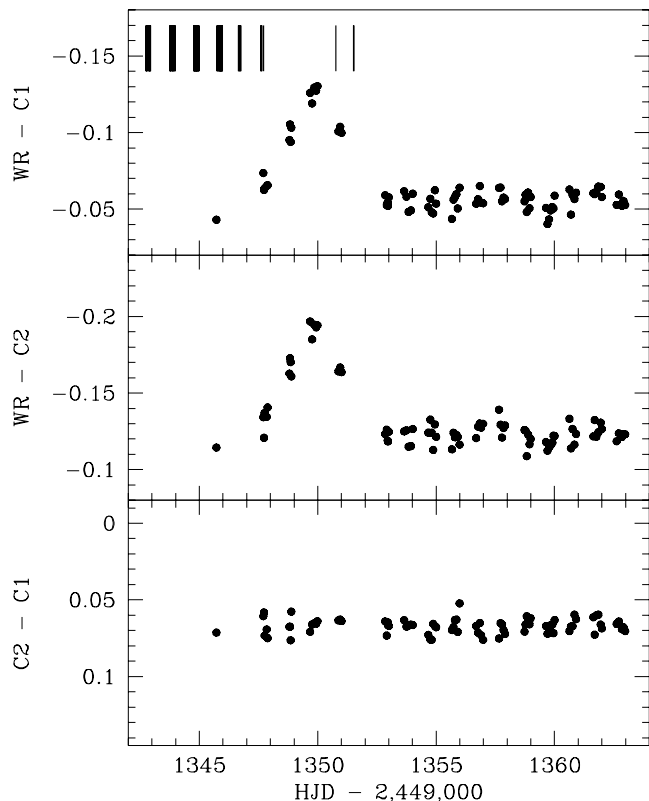


Fig. 1. *Two upper panels:* differential v magnitudes of WR 1 in 1996 September relative to the two comparison stars C1 and C2. *Lower panel:* differential (C2 - C1) magnitudes. Dates when simultaneous spectroscopic observations were performed are indicated by vertical tick lines in the uppermost panel.

data. A periodicity search in the (WR - C1) and (WR - C2) data acquired after HJD 2,450,353 yields no evidence for any periodic signals in the range 6–8 days that would possibly account for the variations observed before this date. The highest peaks in the power spectra of these two datasets (after correction by the CLEAN algorithm; see Roberts et al. 1987) appear (with considerable uncertainty) for periods of about 4 days. However, the significance of these periodic signals is very low and they must thus be regarded as spurious. The periods proposed by Niedzielski (1996a; 2.667 days) and Marchenko et al. (1998a; 11.68 days) are inconsistent with the global light-curve morphology. On the other hand, the periods claimed by Lamontagne (1983; 7.7 days) and Moffat & Shara (1986; 6.1 days) are only consistent with part of the data (before HJD 2,450,353). We will come back to this point later (§4).

3.2. An Overview of the Line-profile Variations

In the following, we will generally illustrate the line-profile variations of WR 1 by means of the strong He II $\lambda 4686$ line

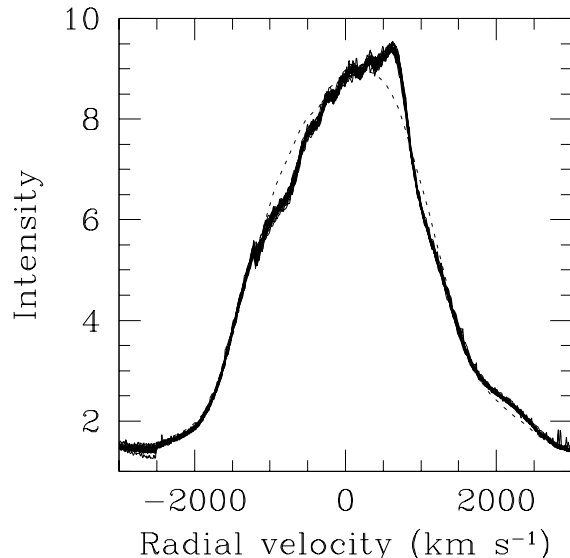


Fig. 2. Superposition of the 21 Echelle spectra acquired on 1996 September 18 (around HJD 2,450,344.873) for the spectral range encompassing He II $\lambda 4686$. These spectra have been obtained on a total time interval of about 5.5 hr. For comparison purposes, the dashed line shows the mean spectrum of the 1996 September dataset. The discontinuities observed at about -2500 km s^{-1} and -1200 km s^{-1} are artefacts of an imperfect connection of the orders. The projected velocities, as everywhere in this paper, are heliocentric and refer to the line laboratory rest wavelength.

as its variations are qualitatively similar to those affecting the other He II features (see §3.5; Niedzielski 1996a). One of the most outstanding features of the line-profile variability is the relatively low level of variability observed within one night.² Such a gradual pattern of variability has been observed whenever several spectra have been obtained during a single night of observation. This phenomenon is illustrated in Figure 2 where we show a superposition of the 21 He II $\lambda 4686$ line profiles obtained on the night of 1996 September 18 (around HJD 2,450,344.873). In sharp contrast, however, noticeable night-to-night variations are observed. This is illustrated in Figure 3 which shows a montage of the nightly mean spectra obtained in 1995 October (*left panel*) and 1996 September (*right panel*) for the spectral region encompassing He II $\lambda 4686$ (it has to be kept in mind that because of the paucity of

² Note that although probably present in WR 1, the small-scale emission-excess features travelling on an hourly timescale on the top of the line profiles (probably induced in WR stars by outwardly moving shocked and/or turbulent material; Lépine & Moffat 1999) cannot be studied here, owing to the insufficient S/N achieved for the Echelle spectra.

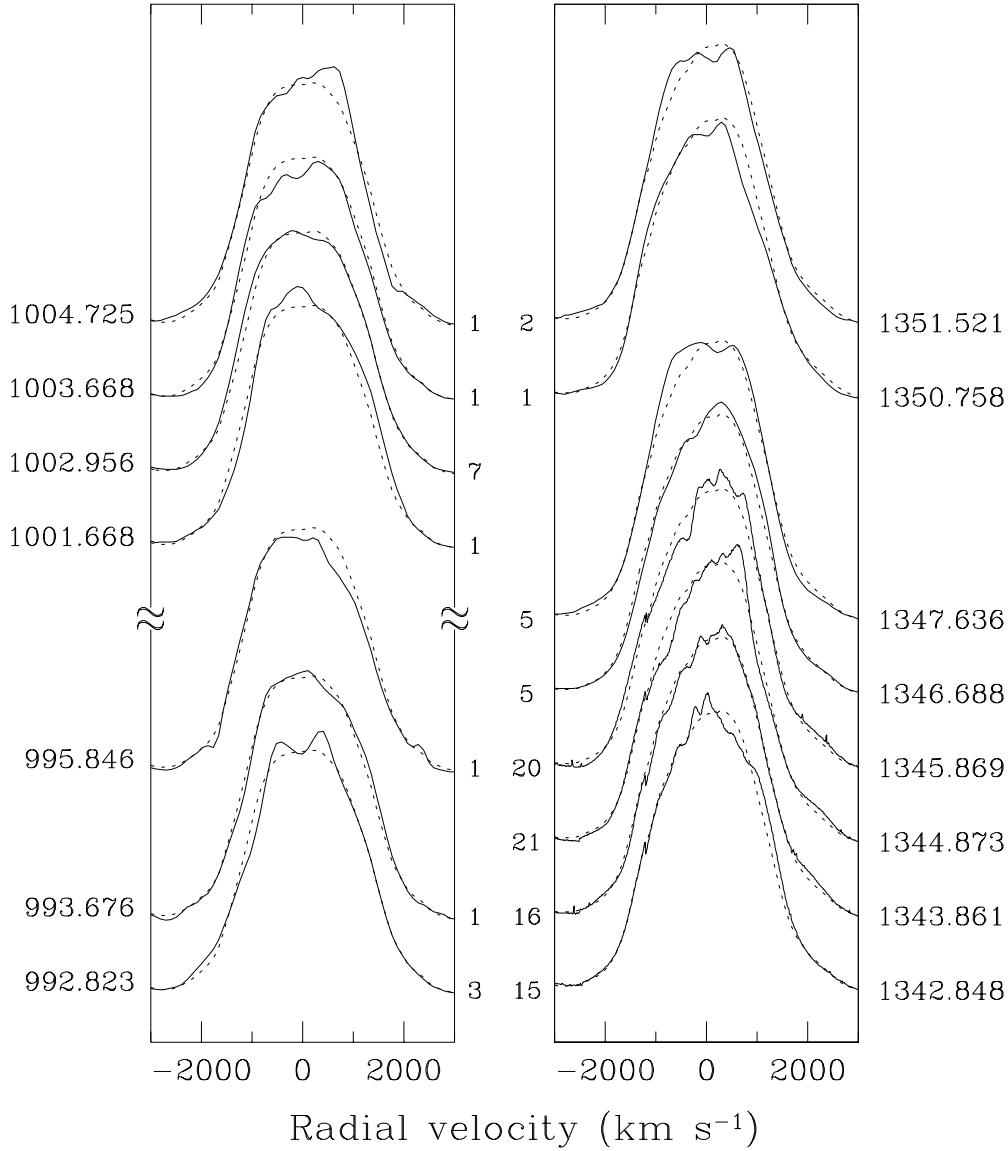


Fig. 3. Montage of the continuum-normalized, nightly mean spectra obtained in 1995 October (*left panel*) and 1996 September (*right panel*) for the spectral range encompassing He II $\lambda 4686$ (the number of individual spectra averaged to form the corresponding nightly mean is indicated between the two panels). The mean heliocentric Julian date of the observations ($-2,449,000$) is indicated on both sides of the panels. For comparison purposes, the unweighted means for 1995 October (7 spectra) and 1996 September (8 spectra) are overplotted as dashed lines. The spectra of consecutive nights are offset by 2.5 units of continuum in the intensity scale.

the photometric data, the strength of the spectral lines in these continuum-normalized spectra has not been corrected for the varying continuum flux level).

3.3. Temporal Variance Spectrum Analysis

The Temporal Variance Spectrum (TVS; Fullerton et al. 1996) has been used to assess the level of spectral variability as a function of wavelength. The (square root of the) TVS, giving the typical “size” of

the deviations from a template-weighted mean spectrum (expressed in percentage of the continuum flux) is shown, along with the 99.0 % confidence level for variability, in Figure 4. As can be seen, highly significant variability affects the emission lines, with the notable exception of N V $\lambda 4945$ for which only little evidence for variability is found. Many peaks (i.e., locations of “preferential” variability) can be distinguished in the TVS. The locations of these peaks (in terms of the projected velocity referred to the laboratory rest wavelength of the spectral feature

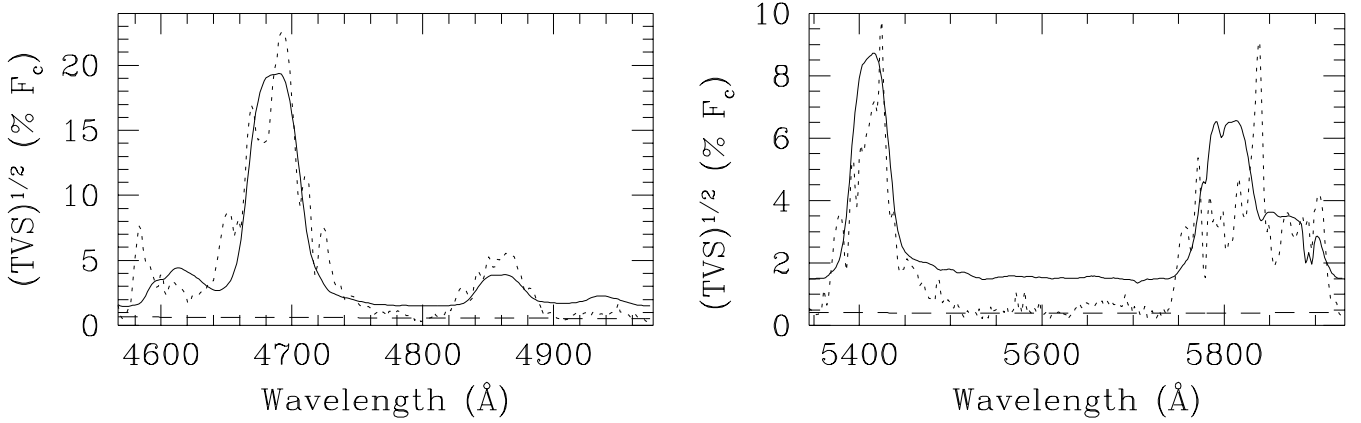


Fig. 4. Square root of the Temporal Variance Spectrum (*short-dashed line*), along with the threshold indicating the 99.0 % confidence level for significant variability (*long-dashed line*). The mean of the spectra used in the calculations is overplotted in arbitrary units (*solid line*).

Table 3. Projected velocities of the TVS subpeaks observed in He II $\lambda 4686$, He II $\lambda 4859$, and He II $\lambda 5412$.^a

He II $\lambda 4686$	He II $\lambda 4859$	He II $\lambda 5412$
– 2260	– 1790	– 1880
– 1060	– 1060	– 1040
	– 550	
+ 430	+ 290	+ 690
+ 1560	+ 1390	+ 1430
+ 2460		

^a In km s^{-1} and referred to the line laboratory rest wavelength.

in question) are quoted in Table 3. This investigation shows that: (a) the variability often extends to velocities comparable to the wind terminal velocity ($v_\infty \approx 2135 \text{ km s}^{-1}$; Rochowicz & Niedzielski 1995), e.g., $v \approx -1790 \text{ km s}^{-1}$ for the relatively unblended line He II $\lambda 4859$; (b) the TVS structure — made up of several subpeaks — presents some similarities for the various He II features. However, the velocities quoted in Table 3 are certainly entangled of considerable uncertainties (e.g., because of blending of TVS subpeaks) making difficult a clear statement as to whether the variability takes place at the same characteristic velocities in different lines.

3.4. The P Cygni Profile Variability

The TVS analysis also reveals substantial variability at the location of the P Cygni absorption component of N V $\lambda 4604$ (Fig. 4). This mainly results from the transition of the N V $\lambda 4604$ feature from a pure emission line-profile in 1995 October to a P Cygni line-profile in 1996 September (Fig. 5). No clear variations in the strength of this absorption trough on a daily timescale are observed.

An enhanced peak in the TVS can also be found at the location where the carbon triplet C IV $\lambda 5806$ and

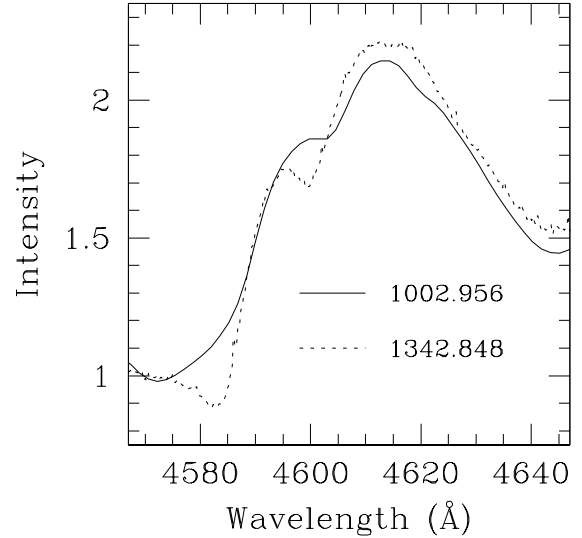


Fig. 5. Superposition for the spectral range encompassing N V $\lambda \lambda 4604, 4620$ of the nightly means of 1995 October 12 (*solid line*) and 1996 September 16 (*short-dashed line*). The mean heliocentric Julian dates of the observations (–2,449,000) are indicated.

He I $\lambda 5876$ merge (Fig. 4). The large daily changes affecting C IV $\lambda 5806$ and/or He I $\lambda 5876$ in October 1995 and September 1996 are illustrated in Figure 6 (this phenomenon is not observed in 1996 November). The high level of variability observed at this particular location is likely due to the superposition of two distinct type of variability: (a) red-wing variability of C IV $\lambda 5806$ as observed in other spectral features (e.g., He II $\lambda 4686$; Fig. 4); (b) variations in the strength of the P Cygni absorption com-

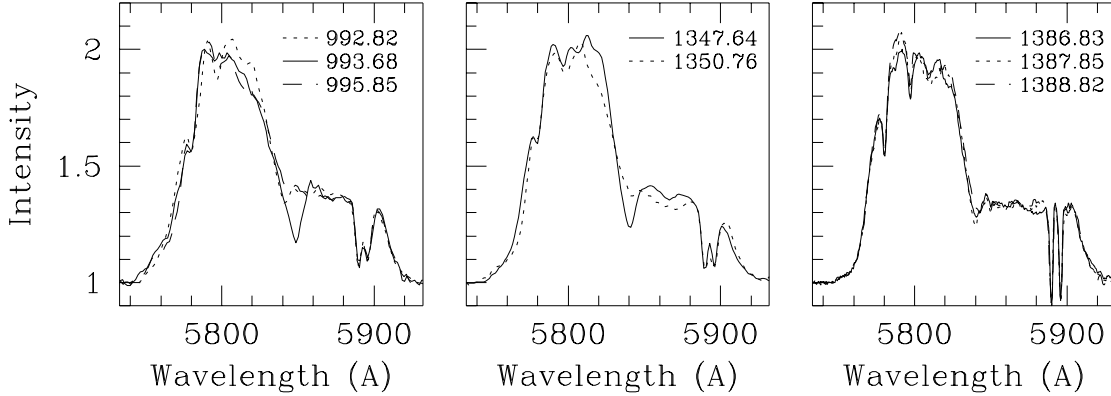


Fig. 6. Superposition for the spectral range encompassing C IV $\lambda 5806$ and He I $\lambda 5876$ of nightly means observed in 1995 October (*left panel*), 1996 September (*middle panel*), and 1996 November (*right panel*). The mean heliocentric Julian dates of the observations ($-2,449,000$) are indicated in each panel.

ponent of He I $\lambda 5876$.³ The latter interpretation is supported by the fact that the projected velocity of the peak in the TVS ($v \approx -1980 \text{ km s}^{-1}$, referred to the He I rest laboratory wavelength) matches fairly well the wind terminal velocity ($v_\infty \approx 2135 \text{ km s}^{-1}$). Considering the relatively modest level of variability affecting the red-wing part of the line profiles in WR 1 (Fig. 4), it is likely that changes in the strength of the P Cygni absorption component of the He I feature *mostly* contribute to the observed changes.

3.5. Correlated Line-profile Variations in Different Lines?

A possible correlated pattern of variability in two different spectral features has been investigated by calculating the Spearman rank-order correlation matrices (see, e.g., Johns & Basri 1995), whose elements $r(i, j)$ yield the degree of correlation between the line intensity variations at pixels i and j in each line profile, respectively. In the case of perfectly, positively correlated variations, a matrix unity is obtained. The correlation matrices of He II $\lambda 5412$ with He II $\lambda 4686$, He II $\lambda 4859$, and N V $\lambda 4945$ are shown in Figure 7 in the form of contour plots, where the lowest contour indicates a significant positive (or negative) correlation at the 99.5 % confidence level (the other spectral lines were not covered enough to be included in the analysis). These matrices are displayed in the projected velocity frame (referred to the line laboratory rest wavelength). A significant positive correlation is generally found between the pattern of variability of He II $\lambda 5412$ and He II $\lambda 4686$. The same conclusion, however restricted to the velocity range $(-1000, +1000) \text{ km s}^{-1}$, holds for

the variations affecting He II $\lambda 5412$ and He II $\lambda 4859$. In contrast, the (weak) variations of N V $\lambda 4945$ are apparently not linked to those of He II $\lambda 5412$ (the same is true for C IV $\lambda 5806$ and He I $\lambda 5876$). Various factors are susceptible to mask a potentially correlated pattern (e.g., noise, blends). Also, due to the stratified nature of WR winds, it is conceivable that (a) two given features present similar, yet time-delayed patterns of variability, and (b) the variability is mainly restricted to the line formation regions of the He II ions and does not extend where the bulk of the N V $\lambda 4945$ emission originates. This would also result in an apparent lack of correlation. Overall, the results of this analysis tend to show that the He II features vary in a fairly similar fashion. The small number of spectral features included in the analysis prevents, however, to draw at this stage more general conclusions.

3.6. Centroid, FWHM, EW, and Skewness Variations

We have investigated the time-dependent changes in the global line-profile properties by calculating the centroid, FWHM, EW, and skewness of He II $\lambda 4686$, the strongest line. The centroid and skewness were calculated as the first moment, and the ratio of the third and the $(3/2)$ power of the second central moments of the portion of the profile above two in units of the continuum (in order to avoid the contribution of blends). The FWHM was determined by a Gaussian fit to the entire line profile. The EWs were calculated by integrating the line flux in the interval 4643–4780 Å. One can note that the mean EW of He II $\lambda 4686$ increased from 313 to 343 Å from 1995 October to 1996 September. This 10 % increase may be explained by an intrinsic EW variability and/or by long-term changes in the stellar continuum flux. As can be seen in Figure 8 (*right panel*), the data obtained in 1996 September generally show *coherent* time-dependent variations. This is especially clear for the skewness time series, with the timescale

³ Such P Cygni absorption troughs of He I $\lambda 5876$ are commonly (and more clearly) observed in other WN stars (e.g., Robert 1992).

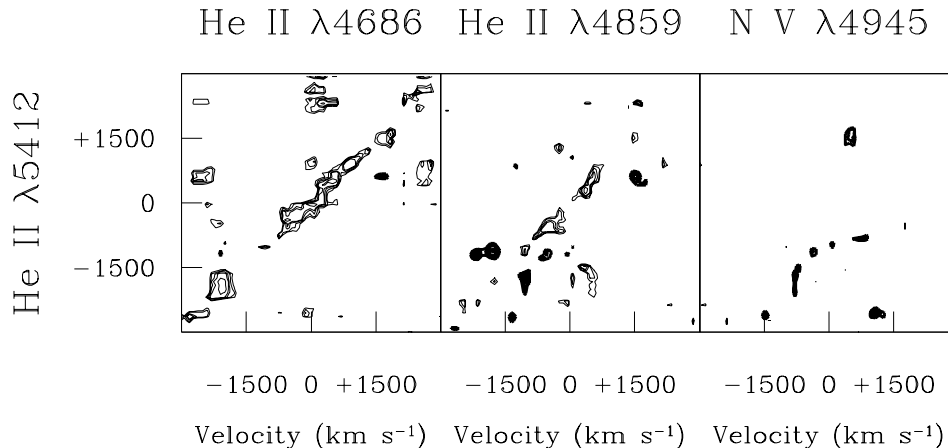


Fig. 7. Correlation matrices of He II $\lambda 5412$ with He II $\lambda 4686$, He II $\lambda 4859$, and N V $\lambda 4945$. Thick and thin contours indicate a negative or positive correlation in the pattern of variability presented by two line profiles at different projected velocities (referred to the line laboratory rest wavelength), respectively. The lowest contour is drawn for a significant correlation at the 99.5 % confidence level.

of the variations being of the same order of magnitude as the variations of the continuum flux shown in the uppermost part of Figure 8, namely, in the range 5–7 days (note that, unlike the EW, the skewness is insensitive to changes in the continuum flux level). On the other hand, however, and although this may be induced by the paucity of the data, no clear time-dependent behavior is noticeable in the 1995 October dataset (*left panel*).

4. Comparison with Previous Studies

Niedzielski (1996a) reported on a spectroscopic pattern of variability of WR 1 very much reminiscent of the one presented by the apparently single WN 5 star WR 6 that displays phase-locked (although strongly epoch-dependent) spectral variations according to $\mathcal{P} \approx 3.77$ days (Morel et al. 1998, and references therein). The results of our investigation of the spectral variability of WR 1 are broadly consistent with this suggestion. In particular, as general features of the spectroscopic pattern of variability, one can note in both objects the substantial variations of the absorption component of the optical P Cygni profiles (readily observable in N V $\lambda\lambda 4604, 4620$ where the absorption trough occasionally disappears; Fig.5) or the coherent time-dependent changes in the global line-profile properties (e.g., skewness; Fig.8). Similarities can also be found with WR 134, another very rare example of single-line WR star displaying cyclical variations (Morel et al. 1999).

Evidence was also presented by Niedzielski (1996a) for cyclical (according to $\mathcal{P} \approx 2.667$ days), correlated changes in the EWs of He II $\lambda 4686$ and He II $\lambda 5412$. The data presented in the present paper do not, however, support a claim of such periodicity. In particular, a period search in our EW data (but also in our centroid, FWHM, and skewness data; Fig.8) yields no significant signal at the

expected frequency. Also, this 2.667 day period can hardly account for our global light-curve morphology (Fig.1). In a speculative vein, this apparent disagreement between our results and those presented by Niedzielski (1996a) *might* point to a multiperiodic nature of the variability in WR 1, with the 2.667 day period being present in 1994–1995 but being dominated by other longer (non)cyclical processes during our observations. It has to be noted that based on a more comprehensive analysis of the data, Niedzielski (private communication) recently questioned the strictly periodic nature of the spectral variations.

As already noted by Niedzielski (1995, 1996b) and Wessolowski & Niedzielski (1996), our data provide evidence for a more gradual spectral pattern of variability than for WR 6; a fact which may imply that the period (*if any*) is longer than 3.77 days. In support of this view, the centroid, EW, and skewness data of He II $\lambda 4686$ show coherent time-dependent patterns of variability (Fig.8), with timescales in the range 5–6 days after a formal periodicity search. However, we caution the reader that this period should not be taken too literally because of the limited time sampling of these data. In particular, a cyclical pattern in this range, as proposed by Lamontagne (1983) and Moffat & Shara (1986), is clearly inconsistent with the lack of continuum flux variations observed after HJD 2,450,353 (Fig.1) unless one invokes a sudden period of “quiescence” after this date, with the small amplitude of the variations masking any periodic patterns.

5. On the Presence of a Companion

Although a cyclical pattern of variability has yet to be unambiguously established in WR 1, general considerations are made below regarding the model assuming an orbiting (unseen) companion as the origin of the variability.

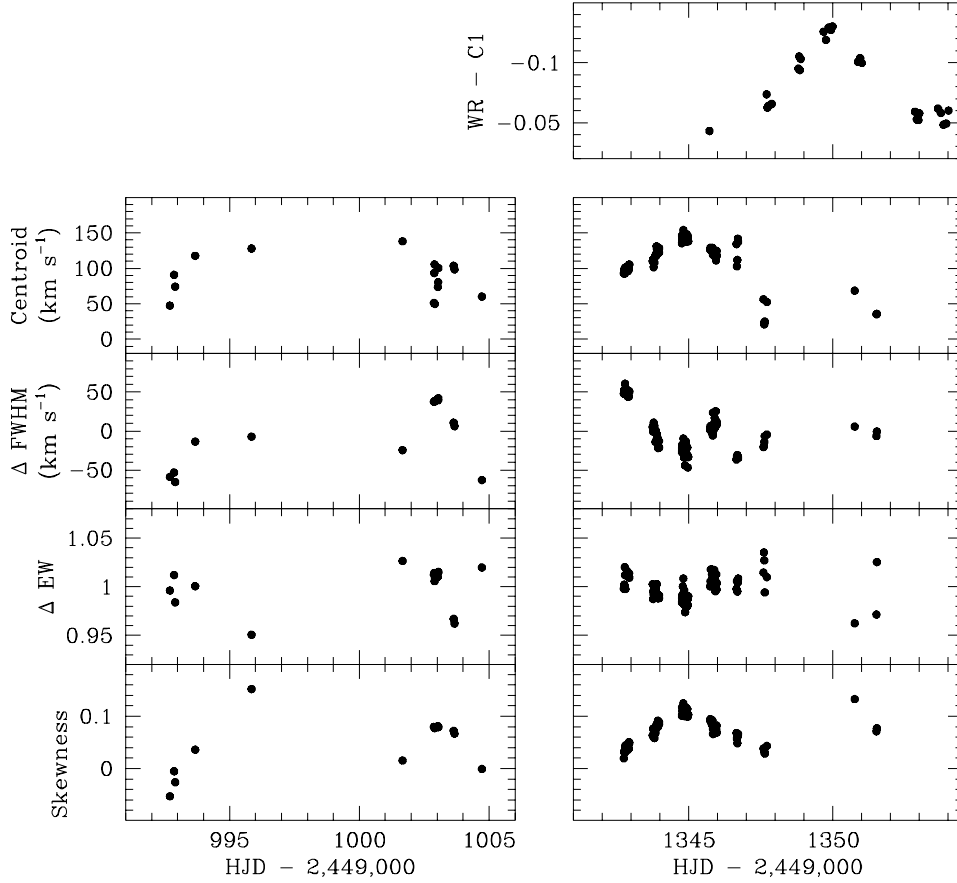


Fig. 8. From top to bottom: continuum flux level variations, centroid variations (in km s^{-1}), deviations of the FWHM around the mean value (in km s^{-1}), EW variations (normalized by division to the mean value), and skewness variations of He II $\lambda 4686$ as a function of the heliocentric Julian date of observation. *Left panel:* 1995 October; *right panel:* 1996 September.

5.1. A Non-degenerate Companion?

Some constraints can be set on the mass, M_* , of this putative companion on the basis of the centroid measurements of He II $\lambda 4686$ presented in Figure 8. Assuming that these variations are *entirely* attributable to orbital motion (i.e., $K_{WR} \approx 70 \text{ km s}^{-1}$), one can explore the allowed values of (P, M_*) . The solid lines in Figure 9 show the result of this investigation for three illustrative values of the orbital inclination ($i = 30^\circ$, 60° , and 90°). In these calculations, we assume a circular orbit and a mass for WR 1 of $9.1 M_\odot$ (Hamann et al. 1995). For a wide range in orbital inclination ($i \gtrsim 30^\circ$) and in orbital period ($P \lesssim 20$ days), an upper limit for the companion's mass of $15 M_\odot$ is derived. Assuming the companion to be a main sequence star, this constrains the spectral type to be later than B1. In this case, the companion's wind is too weak (Grigsby & Morrison 1995) to induce wind-wind collision effects that may induce the large spectral changes

observed in WR 1. For a system observed nearly face-on ($i \lesssim 30^\circ$), larger masses are evidently consistent with the K_{WR} value adopted above. However, no direct evidences (i.e., photospheric lines in the integrated spectrum or dilution of the WR continuum) support the presence of a luminous, early-type companion. In the presence of a non-degenerate companion, one would also expect a flat or eclipsing-type light curve. Yet, the *opposite* behavior is observed in Figure 1. These arguments strongly argue against the presence of a non-degenerate star orbiting WR 1.

5.2. A Collapsed Companion?

For a canonical mass of the companion as a neutron star, $M_* \approx 1.4 M_\odot$, improbably small periods below one day are consistent with the adopted K_{WR} value (Fig.9). However, it has to be kept in mind that the centroid measure-

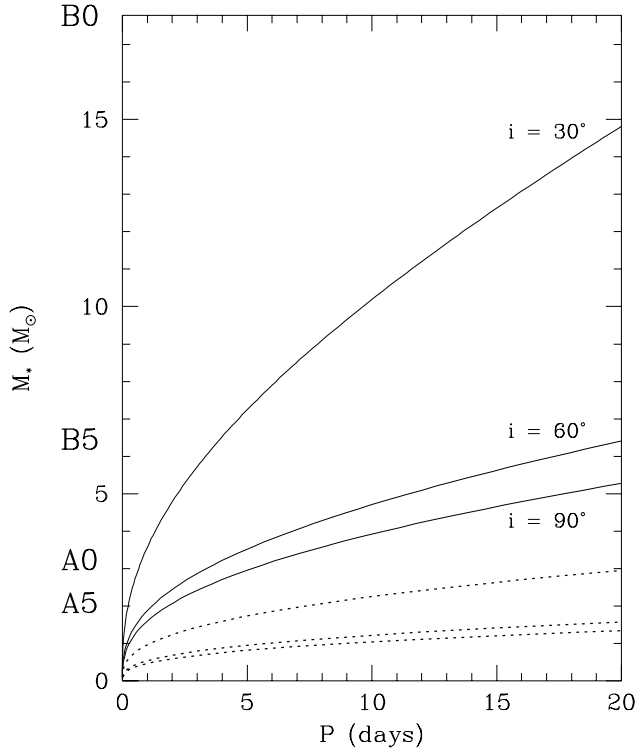


Fig. 9. Allowed values of (P, M_*) when adopting $K_{WR} \approx 70 \text{ km s}^{-1}$ (solid lines) and $K_{WR} \approx 22 \text{ km s}^{-1}$ (short-dashed lines). These values are shown for different orbital inclinations: 30° , 60° , and 90° . The spectral type of the companion (assuming a main-sequence type star) is indicated in the leftmost part of this figure.

ments of He II $\lambda 4686$ included the highly variable uppermost part of the profile which is unlikely to purely reflect orbital motion. Therefore, this K_{WR} value is probably grossly overestimated. If one considers lower K_{WR} values (as Lamontagne 1983: $K_{WR} = 22 \pm 5 \text{ km s}^{-1}$; the allowed values of $[P, M_*]$ are shown in this case by short-dashed lines in Fig.9), much larger periods (as in fact suggested by our study) are allowed. Thus, these considerations are not sufficient by themselves to rule out the presence of a neutron star companion (a black hole companion, on the other hand, would require long periods and/or small orbital inclinations).⁴

In the presence of a collapsed companion, one may expect fairly strong, accretion-type X-ray emission. Earliest observations by the *HEAO A-1* experiment gave an upper limit $L_X \approx 4.4 \times 10^{33} \text{ erg s}^{-1}$ on the emission in the 0.5–20 keV range (Helfand 1980). A value $L_X = 7.07 \pm 2.85 \times 10^{32} \text{ erg s}^{-1}$ in the 0.2–2.4 keV range has been reported for WR 1 during the *ROSAT* all-sky survey

(Pollock et al. 1995). WR 1 is a fairly strong X-ray emitter compared to other (apparently) single WN stars. However, its emission is by no means unusual when only considering the WNE-s subclass (Wessolowski 1996). Two subsequent pointed *ROSAT* PSPC observations showed that a satisfactory fit to the X-ray spectrum can be achieved, either with a *Raymond-Smith* thermal plasma of about 1 keV or by the model developed by Baum et al. (1992), assuming a mixture of “cool” (in radiative equilibrium) and “hot” (shocked) material (Wessolowski et al. 1995; Wessolowski 1996). This picture is consistent with our current understanding of the X-ray production in bona fide single WR stars, as being due to radiatively-induced instabilities (e.g., Willis & Stevens 1996). This “normal” level of X-ray emission from WR 1 does not constitute, however, a decisive argument against the presence of a collapsed companion, as the accretion of the wind material onto the neutron star is known to be inhibited in some X-ray binaries (e.g., Zhang et al. 1998).

Because of the spiral-in process that massive close binaries are believed to experience in the course of their evolution, one is led to expect periods of some hours for systems made up of a WR star and a compact companion, not days (e.g., De Donder et al. 1997). A period of 4.8 hr is observed in Cygnus X-3, the prime candidate for a WR + compact companion system (van Kerkwijk et al. 1996).

6. Concluding Remarks

The single-star hypothesis appears appealing when considering the similarities between the optical spectral pattern of variability of WR 1 and the ones of the two peculiar stars WR 6 and WR 134. In this respect, although the light-curve morphology of WR 1 (a “bump” followed by a plateau) has, to our knowledge, no example among the WR population (Moffat & Shara 1986; Lamontagne & Moffat 1987; Antokhin et al. 1995; Marchenko et al. 1998b), such a well-defined light-curve pattern is reminiscent of what is observed in WR 6 (Robert et al. 1992).⁵ Such a repeatable pattern would, however, imply an unlikely large value for the period in the context of this single-star hypothesis ($P \gtrsim 18$ days).

Since the substantial depolarization of the emission lines observed in WR 6 and WR 134 is generally taken as evidence for an equatorially-enhanced outflow (Schulte-Ladbeck et al. 1991, 1992), revealing the same phenomenon in WR 1 may lead to the interesting suggestion that the occurrence of large-scale line-profile and photometric variations (and thus possibly of azimuthally structured outflows) in single WR stars is somehow linked to the existence of a wind-compressed zone (Ignace et al. 1996).

⁴ Considering a lower K_{WR} value in §5.1 does not qualitatively modify our conclusions.

⁵ Curiously, a very similar light-curve morphology (both in terms of the timescales involved and of the amplitude of the variations) has been noticed in the Be star FV CMa (Balona et al. 1992).

Acknowledgements. We acknowledge an anonymous referee and Alex W. Fullerton, whose comments have stimulated a substantial improvement of this manuscript. T. M., Y. G., and N. S.-L. wish to thank the Natural Sciences and Engineering Research Council (NSERC) of Canada and the Fonds pour la Formation de Chercheurs et l'Aide à la Recherche (FCAR) of Québec for financial support; T. E. is grateful for full financial aid from the Evangelisches Studienwerk/Germany, which is supported by the German Government.

References

- Antokhin, I., Bertrand, J.-F., Lamontagne, R., Moffat, A. F. J., Matthews, J. 1995, *AJ*, 109, 817
- Balona, L. A., Cuypers, J., & Marang, F. 1992, *A&AS*, 92, 533
- Baum, E., Hamann, W. -R., Koesterke, L., & Wessolowski, U. 1992, *A&A*, 266, 402
- De Donder, E., Vanbeveren, D., & van Bever, J. 1997, *A&A*, 318, 812
- Firmani, C., Koenigsberger, G., Bisiacchi, G. F., Moffat, A. F. J., & Isserstedt, J. 1980, *ApJ*, 239, 607
- Fullerton, A. W., Gies, D. R., & Bolton, C. T. 1996, *ApJS*, 103, 475
- Fullerton, A. W., Massa, D. L., Prinja, R. K., Owocki, S. P., & Cranmer, S. R. 1997, *A&A*, 327, 699
- Grigsby, J. A., & Morrison, N. D. 1995, *ApJ*, 442, 794
- Hamann, W.-R., Koesterke, L., & Wessolowski, U. 1995, *A&A*, 295, 151
- Harries, T. J., Howarth, I. D., Schulte-Ladbeck, R. E., & Hillier, D. J. 1999, *MNRAS*, 302, 499
- Helfand, D. J. 1980, *PASP*, 92, 691
- Ignace, R., Cassinelli, J. P., & Bjorkman, J. E. 1996, *ApJ*, 459, 671
- Johns, C. M., & Basri, G. 1995, *AJ*, 109, 2800
- Kaper, L., et al. 1997, *A&A*, 327, 281
- Lamontagne, R. 1983, Ph.D. Thesis, Univ. Montréal
- Lamontagne, R., & Moffat, A. F. J. 1987, *AJ*, 94, 1008
- Lépine, S. 1998, Ph.D. Thesis, Univ. Montréal
- Lépine, S., & Moffat, A. F. J. 1999, *ApJ*, 514, 909
- Levine, S., & Chakrabarty, D. 1995, IA-UNAM Technical Report #MU-94-04
- McCandliss, S. R., Bohannan, B., Robert, C., & Moffat, A. F. J. 1994, *Ap&SS*, 221, 155
- Marchenko, S. V., et al. 1998a, *A&A*, 331, 1022
- Marchenko, S. V., Moffat, A. F. J., Eversberg, T., Hill, G. M., Tovmassian, G. H., Morel, T., & Seggewiss, W. 1998b, *MNRAS*, 294, 642
- Moffat, A. F. J., & Shara, M. M. 1986, *AJ*, 92, 952
- Morel, T. 1998, Ph.D. Thesis, Univ. Montréal
- Morel, T., St-Louis, N., Moffat, A. F. J., Cardona, O., Koenigsberger, G., & Hill, G. M. 1998, *ApJ*, 498, 413
- Morel, T., et al. 1999, *ApJ*, 518, 428
- Niedzielski, A. 1995, in *Proc. IAU Symp. 163, Wolf-Rayet Stars: Binaries, Colliding Winds, Evolution*, ed. K. A. van der Hucht & P. M. Williams (Dordrecht: Kluwer), 52
- Niedzielski, A. 1996a, in *Proceedings of the 33rd Liège International Astrophysical Colloquium*, ed. J. M. Vreux et al., 277
- Niedzielski, A. 1996b, in *Proceedings of the 27th Meeting of the Pol. Astron. Soc.*, 98
- Niedzielski, A. 1998, *Acta Astron.*, 48, 729
- Pollock, A. M. T., Haberl, F., & Corcoran, M. F. 1995, in *Proc. IAU Symp. 163, Wolf-Rayet Stars: Binaries, Colliding Winds, Evolution*, ed. K. A. van der Hucht & P. M. Williams (Dordrecht: Kluwer), 512
- Robert, C. 1992, Ph.D. Thesis, Univ. Montréal
- Robert, C., et al. 1992, *ApJ*, 397, 277
- Roberts, D. H., Lehár, J., & Dreher, J. W. 1987, *AJ*, 93, 968
- Rochowicz, K., & Niedzielski, A. 1995, *Acta Astron.*, 45, 307
- Schulte-Ladbeck, R. E., Nordsieck, K. H., Taylor, M., Nook, M. A., Bjorkman, K. S., Magalhães, A. M., & Anderson, C. M. 1991, *ApJ*, 382, 301
- Schulte-Ladbeck, R. E., Nordsieck, K. H., Taylor, M., Bjorkman, K. S., Magalhães, A. M., & Wolff, M. J. 1992, *ApJ*, 387, 347
- Smith, L. J., & Willis, A. J. 1994, *Ap&SS*, 221, 189
- van Kerkwijk, M. H., Geballe, T. R., King, D. L., van der Klis, M., & van Paradijs, J. 1996, *A&A*, 314, 521
- Vreux, J.-M., Gosset, E., Bohannan, B., & Conti, P. S. 1992, *A&A*, 256, 148
- Wessolowski, U., Hamann, W. -R., Koesterke, L., Hillier, D. J., & Puls, J. 1995, in *Proc. IAU Symp. 163, Wolf-Rayet Stars: Binaries, Colliding Winds, Evolution*, ed. K. A. van der Hucht & P. M. Williams (Dordrecht: Kluwer), 174
- Wessolowski, U. 1996, in *Proceedings of the 33rd Liège International Astrophysical Colloquium*, ed. J. M. Vreux et al., 345
- Wessolowski, U., & Niedzielski, A. 1996, in *Proc. Röntgenstrahlung from the Universe*, ed. Zimmermann, H. U., Trümper, J., & Yorke, H., MPE Report, 263, 73
- Willis, A. J., & Stevens, I. R. 1996, *A&A*, 310, 577
- Zhang, S. N., Yu, W., & Zhang, W. 1998, *ApJ*, 494, L71